Large-Scale Additive Manufacturing of Self-Heating Molds

Kazi Md Masum Billah[1,2], Jesse Heineman[1], Parithosh Mhatre[1], Alex Roschli[1], Vipin Kumar[1], Seokpum Kim[1], Gregory Haye[3], Jerry Jackson[3], Zach Skelton[3], Vlastimil Kunc[1], Ahmed Arabi Hassen[1,*]

[1]Manufacturing Science Division (MSD), Oak Ridge National Laboratory (ORNL), Knoxville, TN 37932, USA

[2]Department of Mechanical Engineering, The University of Texas at El Paso, El Paso, TX, USA

[3]Advanced Materials Group, Airtech, Huntington Beach, CA, USA

[*] Corresponding author: Email: hassenaa@ornl.gov, Tel: (205) 470-4010

Abstract

Large-scale material extrusion additive manufacturing technology is becoming the new mainstream technology for scaled-up composite mold and die applications. This paradigm shift in composite processing technology is primarily driven by out-of-autoclave tooling applications, in which fiber reinforced composite molds with scaled-up sizes and embedded heating elements are attractive. The present research describes the design, manufacture, and testing of self-heating composite molds fabricated via a large-scale pellet extrusion 3D printing machine with an integrated wire co-extrusion tool. Polycarbonate (PC) composites reinforced with carbon fiber (PC/CF; 20 wt.%) and glass fiber (PC/GF; 20 wt.%) were used to fabricate molds. Joule heating thermal test results showed that uniform temperatures (~100°C) were achieved for both PC/CF and PC/GF mold surfaces, using a custom-made feedback control power supply and infrared thermography. Mechanical characterizations, including tensile and flexural testing, were performed on the wire-embedded and un-wired PC/CF and PC/GF base specimens to investigate the impact of the fiber reinforcement as well as the embedded wires. In the direction of extrusion, the ultimate tensile stress of PC/CF was 105 MPa, and that of PC/GF was 73 MPa, while the neat PC value was 64 MPa. Inner-bead voids and interfacial gaps were observed and characterized via optical and scanning electron microscopy. The embedded wires and inner bead voids negatively affected the mechanical properties of the composites. However, the stiffness of the wire-embedded mold was still satisfactory, proving that this technology can be used to fabricate additively manufactured out-of-oven/autoclave molds.

1. Introduction

The development of high-performance fiber reinforced polymer composites brought a revolution in the polymer-based manufacturing community. Their higher strength-to-weight ratio, mechanical reinforcement, improved thermal & electrical conductivity, and multifunctional applications greatly benefited the automotive, renewable energy, and aerospace manufacturing industries [1]–[5]. Decade-long research and development activities made it possible to develop state-of-the-art fiber-reinforced high-performance polymer composite manufacturing technology, namely autoclave processing [6], [7]. The sequential construction of Boeing's autoclave vessel, which has been used to manufacture the entire wingspan (71.6 m in length) of the 777-X aircraft since 2014, is the perfect example of the recent progress in autoclave processing technology [8], [9]. The autoclave curing process involves material layup on a rigid mold, followed by heating in an oven under pressure (typically 10 to 20 bar). The pressures and temperatures achieved by the autoclave curing process produce fiber-reinforced net shape and high-quality parts with low void contents. Undoubtedly, the autoclave process is a well-developed and reliable method of manufacturing high-performance composite structures. However, some of the disadvantages of the autoclave process are hindering the growth of the small - to mid-size composite tooling industries and causing existing business to shift from the United States to other territories of the world [10]. The disadvantages of autoclave processing are: (a) high capital costs, (b) a high labor intensity, (c) long cycle times, (d) a high ratio of operating cost to part size, (e) parts with internal cavities require complex tooling and bagging, (f) inefficient conduction heating, and (g) high energy consumptions [11], [12] just to list a few. This warranted the continued pursuit of processes with characteristics such as efficient heating, faster cycle times, and lower labor intensities. Undeniably, out-of-autoclave (OOA) processing was able to resolve some of those issues, for instance, it reduced the initial cost and decreased cycle time.

OOA processing technology refers to the process of fabricating composite structures via vacuum-assisted consolidation while still producing autoclave-quality parts. In brief, the OOA process consists of making the mold, laying down the prepreg, vacuuming to remove voids, consolidating the prepreg fiber system, curing of the resin while heating in an oven, post-curing heating, and finally removing the final part from the mold [13]. While the OOA process reduces the acquisition and operating costs compared to its autoclave counterpart, the use of an inefficient heating mechanism (thermal oven) still leaves room to further improve and reduce the cost of operation.

Therefore, an efficient heating method, such as an embedded heating element in the OOA mold, is paramount for the adoption of this technology in the high-performance composite manufacturing industry.

Material extrusion additive manufacturing (AM) in large scale is becoming a mainstream technology for the fabrication of scaled-up composite molds with reduced costs, lead times, and cycle times compared to traditional autoclave tooling [10], [14], [15]. The Big Area Additive Manufacturing (BAAM) system at the Oak Ridge National Laboratory (ORNL) has successfully demonstrated the use of fiber-reinforced thermoplastic-based composite pellet extrusion to manufacture autoclave molds [10], [14]. The transition from traditional manufacturing methods to AM reduced the cost to fabricate autoclave molds by 10-100 times (based on the size: ≥$100,000 to ~$5,000) and reduced the amount of time from conceptual design to the final tool by an order of magnitude (from months to weeks). Although the thermal conductivity of the fiber-reinforced composite was improved marginally (0.177 $W \cdot m/K$ for ABS and 0.397 $W \cdot m/K$ for 13 wt.% CF reinforced ABS measured along the deposition direction, and 0.156 $W \cdot m/K$ measured perpendicular to the deposition direction) [16], heating of the printed autoclave molds using an oven remained on the list of expensive items. Therefore, manufacturing of OOA molds using the BAAM system becomes a potential solution for energy-efficient manufacturing.

Considering the fabrication of an embedded and self-heated OOA composite mold, the BAAM system is equipped with a wire co-extrusion technology. The integrated wire co-extrusion tool in the BAAM system allows the embedding of a resistive heating wire, such as nichrome wire, within the printed part. A detailed description of the wire coextrusion tool design and integration within the BAAM system was presented in [17], [18]. The embedding of resistance wire (nichrome) in each layer of deposited materials during 3D printing adds a new area of research in the OOA tooling manufacturing community.

This research paper investigated the pioneering yet exploratory manufacturing method of self-heated OOA composite molds, using the BAAM system. Two different composite materials were chosen for fabrication of wire-embedded and self-heating composite molds. Thermal testing was performed to characterize the temperature uniformity over the mold panel surface. Mechanical characterizations were performed to investigate the impact of the embedded heating wire as well as the effect of the fiber loading in the composites. Considering the mechanical [19] and thermal

[20] anisotropy of the BAAM-printed parts, the mechanical properties of the printed mold were evaluated and recommendations for future improvement are made. The authors believe that utilizing the developed technology to manufacture self-heated molds will reduce the capital expenditures and manufacturing bottlenecks in the composite manufacturing industry.

2. Methodology

2.1 Wire Co-Extrusion System

The BAAM 3D-printing machine was equipped with a wire coextrusion tool to fabricate wire embedded structures. Figure 1 represents the integrated wire coextrusion tool on the BAAM system. The three main parts of the system are (a) the extruder, (b) the coextrusion tool, and (c) the extrusion nozzle, with a tamper. Details of the system, tool design, and software integration were discussed in [18], and [21]. However, a brief description of the system is provided here. The build volume of the BAAM system is 6 m (20 ft) × 2.44 m (8 ft) × 1.83 m (6 ft). The extruder has the ability to deposit up to 50 kg/h (~100 lb/h) of material and was equipped with an extrusion nozzle of 7.62 mm (0.3 in) diameter. For the wire coextrusion tool, 24 AWG nichrome wire was used as a resistance heating element to embed within the extruded beads.

2.2 Sample Preparation

2.2.1 Materials

In this research, two different types of thermoplastic composite pellets were used for experimental investigation: Polycarbonate with 20 wt.% carbon fiber loading (PC/CF) and polycarbonate with 20 wt.% glass fiber loading (PC/GF) (Techmer PM LLC (Clinton, TN, USA)), as listed in Table 1. Both materials were dried for four hours at 90°C using a dryer (Dri-Air Industries Inc., East Windsor, CT, USA). A nichrome alloy wire with Nickel 60%, Chromium 16%, and Iron 24%, and a diameter of 0.508 mm with electrical resistivity of 0.126 ohms-m (McMaster-Carr, Cleveland, OH, USA) was used during the co-extrusion process.

Table 1. Thermoplastic composite materials used for experimental and mold fabrication

Resin	**Fiber (wt.%)**	**Manufacturer**	**Product Name**
Polycarbonate	CF (20)	Techmer PM LLC	Electrafil ® PC 1501 3DP
Polycarbonate	GF (20)	Techmer PM LLC	Hifill ® PC 1903 ECO 3DP

2.2.2 Hexagon Printing and Sample Harvesting

Single-bead wall hexagons were printed using the BAAM system to fabricate the tensile and flexural testing specimens. Hexagons were printed using a continuous printing technique called spiralizing. Therefore, there was no seam within the printed hexagon. The layer height was 3.81 mm, and the layer width was 13 mm. The printing parameters for the hexagons are listed in Table 2. In the case of wire-embedded hexagon printing, the wire feeding rate was adjusted manually with a custom-made LabView controller, until it matched the gantry speed. This adjustment was calibrated visually by watching for when the wire was neither being pulled out of the bead, nor being pushed in excessively, which causes it to protrude out of the side of the bead. After printing the hexagons, surface finishing was done by performing a milling operation using a computer numerical control (CNC) machine. Material was removed equally from both sides of the hexagon and the final thickness was reduced to 6.4 mm from the printing wall thickness of 13 mm.

Tensile and flexural testing samples were harvested along the X and Z-axis direction according to the ASTM D638 Type-I and ASTM D790 specimen dimensions, as shown in Figure 2, where the X-axis is in the direction of the deposition and Z-axis is perpendicular to the deposition direction (direction of the interface). For the flexural specimens only, the sample thickness was further reduced to 3.2 mm by machining. Five specimens were harvested in each direction for both PC/CF

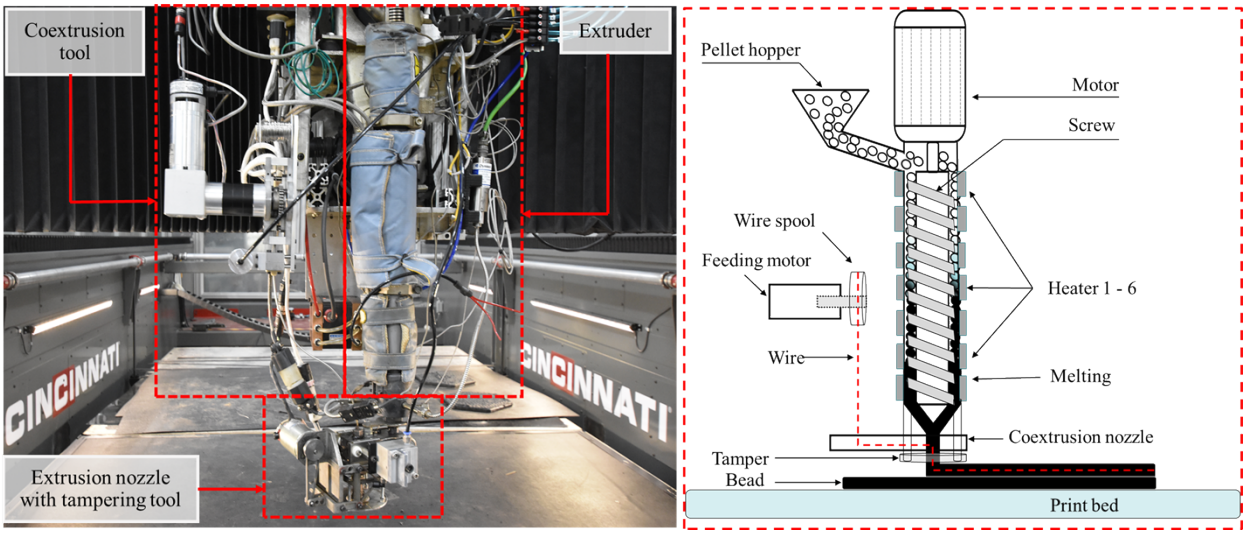

Figure 1. (a) Integrated wire coextrusion tool and extruder mounted on BAAM gantry and (b) Schematic of the BAAM single screw extruder with wire co-extrusion system.

and PC/GF parts. For comparison, neat PC/CF and PC/GF specimens, which did not contain the embedded heating wires, were harvested from two separately printed parts, also fabricated on the BAAM system with similar printing parameters. The authors would like to direct the attention of readers to the use of the terms “neat PC/CF” and “neat PC/GF”, which here refer to un-wired specimens that are still reinforced with chopped CFs and GFs, respectively.

Table 2. Extrusion parameters used in BAAM to extrude fiber-reinforced thermoplastic composites

Material	Heater 1 (°C)	Heater 2 (°C)	Heater 3 (°C)	Heater 4 (°C)	Heater 5 (°C)	Heater 6 (°C)	Melt (°C)	Extrusion speed (rpm)	Gantry speed (mm/s)
PC/GF	200	215	230	230	230	230	235	50	100
PC/CF	200	220	240	240	240	240	240	50	100

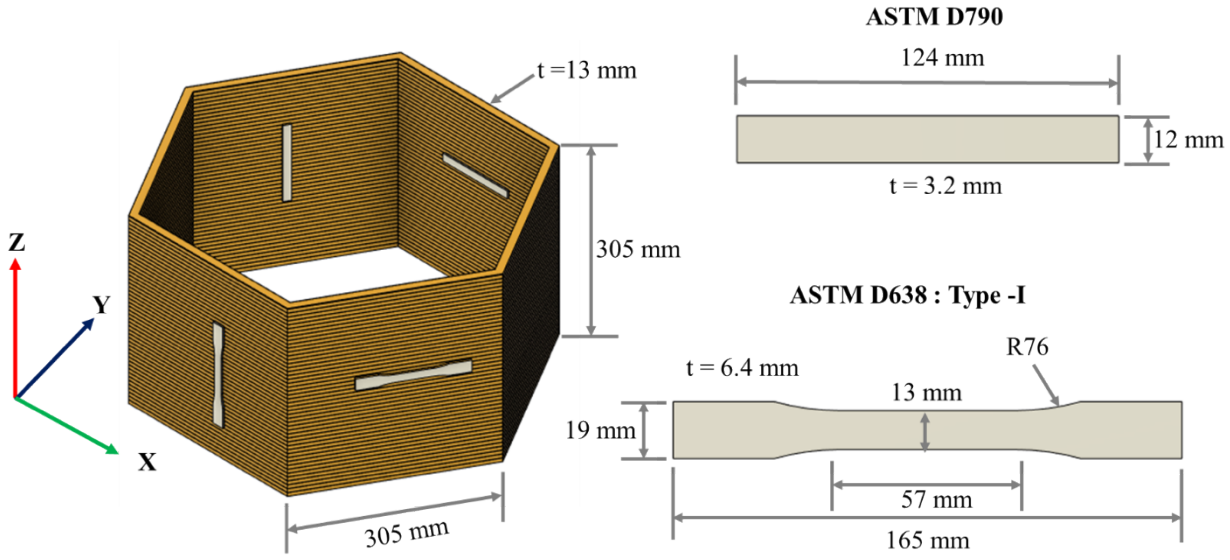

Figure 2. Schematic for the hexagon printed and dimensions for samples used in the mechanical characterization. Five specimens were harvested in each direction.

2.3 Manufacturing of the Self Heating Mold

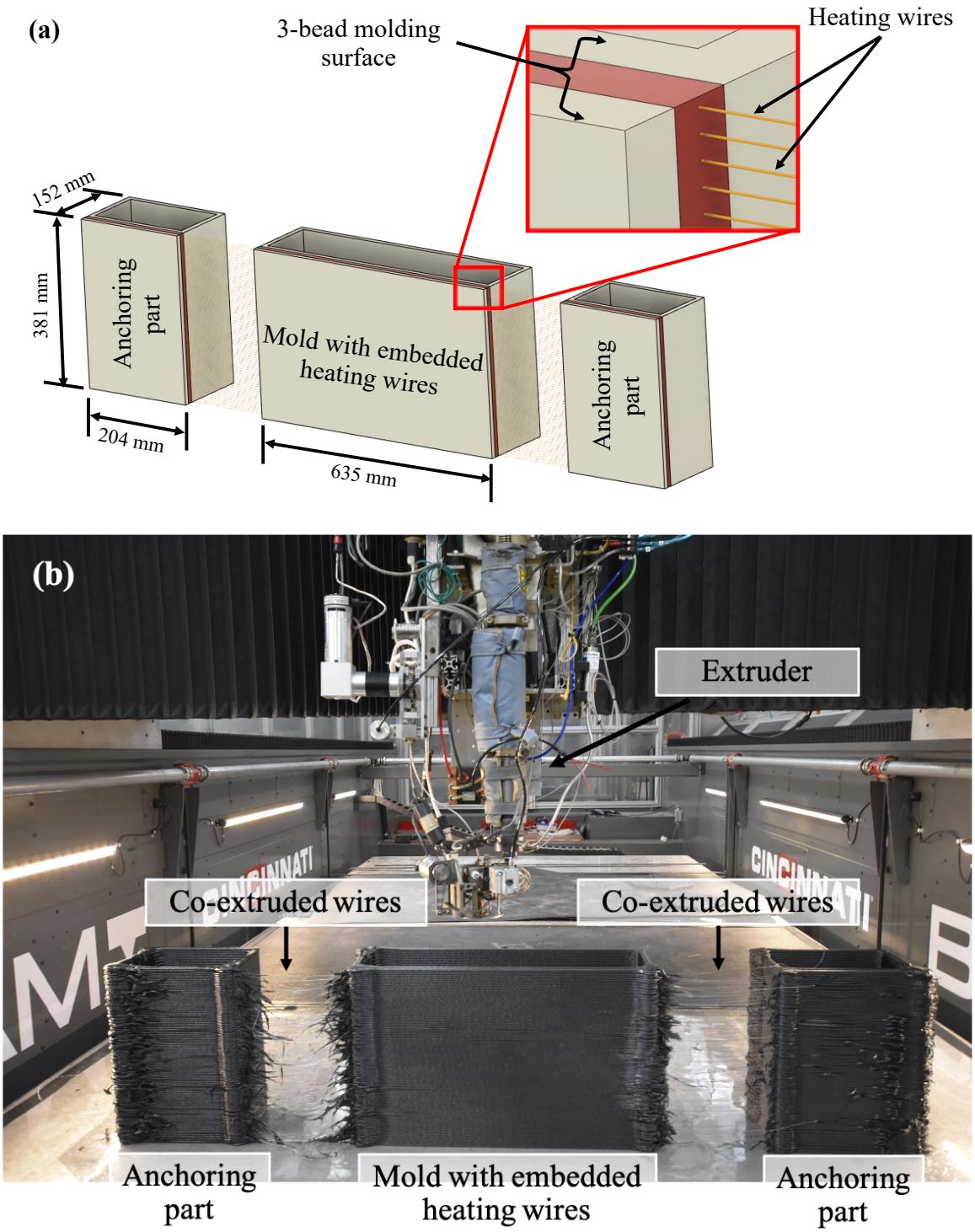

Figure 3. AM self-heated mold with embedded heating wire; (a) schematic for the mold and sacrificial anchoring parts dimensions, and (b) actual PC/CF composite mold with embedded wires during printing on the BAAM system.

For the experimental investigation of OOA molds fabricated by the BAAM system, two self-heating molds were fabricated using either PC/CF or PC/GF. The schematic of the mold is shown in Figure 3(a). It can be noticed in Figure 3(a) that the mold had two rectangle pieces on each side (sacrificial parts); these were used to anchor the wires and avoid wire entanglement during the printing process. The mold itself had a molding surface with a wall thickness of 39 mm, i.e., it consisted of three beads, while the other walls (support structures) had thicknesses of only 13 mm, i.e., all other walls were single bead. Of the three molding surface beads, heating wires were only coextruded within the middle bead. The reason for choosing three beads for the molding surface (front wall) was to ensure there was enough material for the machining done to finish the surfaces of both faces. The wall thickness of the molding surface was 25 mm after the machining was performed.

2.4 Mechanical Characterization

2.4.1 Tensile Testing

For the mechanical characterizations, prior to testing, samples were stored in a custom-made humidity control chamber at a temperature of 23 $\pm$ 3 °C and relative humidity of 50 $\pm$ 5 %. Tensile testing was performed according to the ASTM D638, using a universal tensile testing machine, an MTS (MTS systems corporation, Eden Prairie, MN, USA) 647 hydraulic wedge grips with a 4450 N load cell and a 200 k micro-strain extensometer (MTS Model 632, 31E-24). At least five specimens from each condition were tested to failure at a rate of 1.5 mm/min, and data was collected at a rate of 10 Hz using a custom-made LabVIEW VI.

2.4.2 Flexural Testing

Three-point bending or flexural testing on the neat and wire-embedded PC/CF and PC/GF specimens were performed in a SATEC Systems Instronis (Norwood, MA, USA) machine as per the ASTM D790 standard. The crosshead was maintained constant at 1.35 mm/min and support span length was adjusted by the span length-to-width ratio of 32:1. The loading nose diameter was 10 mm and the diameter of the supports nose was 10 mm. During the testing, the sample support span was 20 mm. The flexural stress and modulus of elasticity during bending were evaluated. Five single specimen experiments were performed for each sample group and the average values were reported for analysis.

2.5 Optical Characterization

Optical microscopy of the wire-embedded composite specimens was performed using a benchtop microscope to visualize the embedded wires and the intra-bead voids in printed parts. Samples were harvested from the tensile testing specimen's gauge length section and were polished. Analysis via scanning electron microscopy (SEM) allowed for an understanding of the interfaces between the integrated wire and the printed composites. Fractured surfaces of the wire-embedded tensile testing specimens were examined using a Zeiss Evo 15 SEM (Carl Zeiss Microscopy, LLC, White Plains, NY, USA), operated with an accelerating voltage of 5 kV and probe current of 5 nA.

2.6 Thermal Characterization

The wire-embedded mold was heated using the Joule Heating Principle, which is also known as resistance heating [22]. Thermal characterization of the mold heating effect was created by delivering electrical power using the following formula:

$$P = VI = I^2R \qquad \text{Eq. (1)}$$

where V is the terminal voltage in (Volts), I is the current (Amps), R is the resistance of the wire (Ohms), and P is the input power (Watts). Mold heating can be done in multiple ways, such as selectively heating desired areas or heating the entire molding surface. In this research, we presented both configurations of heating using the custom-made power supply. The challenge of resistance heating the mold was non-uniform heating, which is not desirable for most of the autoclave/oven tooling processes. Thus, a custom-made feedback control system was developed to control as well as adjust the heating uniformity.

The custom-made power supply was designed to provide an equal amount of direct current (DC) of 10A as well as maintain a voltage difference of 24VDC within the terminal. The power supply setup consisted of a multi-zone temperature control system. The system controlled the duty cycle of the power supplied to the mold zones based on feedback from respective thermocouples, to achieve the user-specified setpoints. The control system consisted of the following components: (a) OMEGA universal 6 channel controllers, (b) a CN611A programmable controller, (c) a solid state relay, (d) k-type thermocouples, and (e) a 24V and 480W power supply. The OMEGA universal controller was programmable with independent parameters for each of the zones. The resulting system could control five zones with a maximum power of 240W per zone. A typical control loop for a zone is shown in Figure 4. The PID gains were obtained by running autotune for

one zone and then using those values for all the zones. The mold surface was monitored using an infrared (IR) camera (FLIR Systems, Inc., Wilsonville, OR, USA) during the entire duration of each test. Each mold was heated for 2 hours. During the first hour, the mold was heated with a setpoint of 100°C. During the second hour, the setpoint was adjusted manually to provide the most even temperature profile on the mold surface, according to the IR camera.

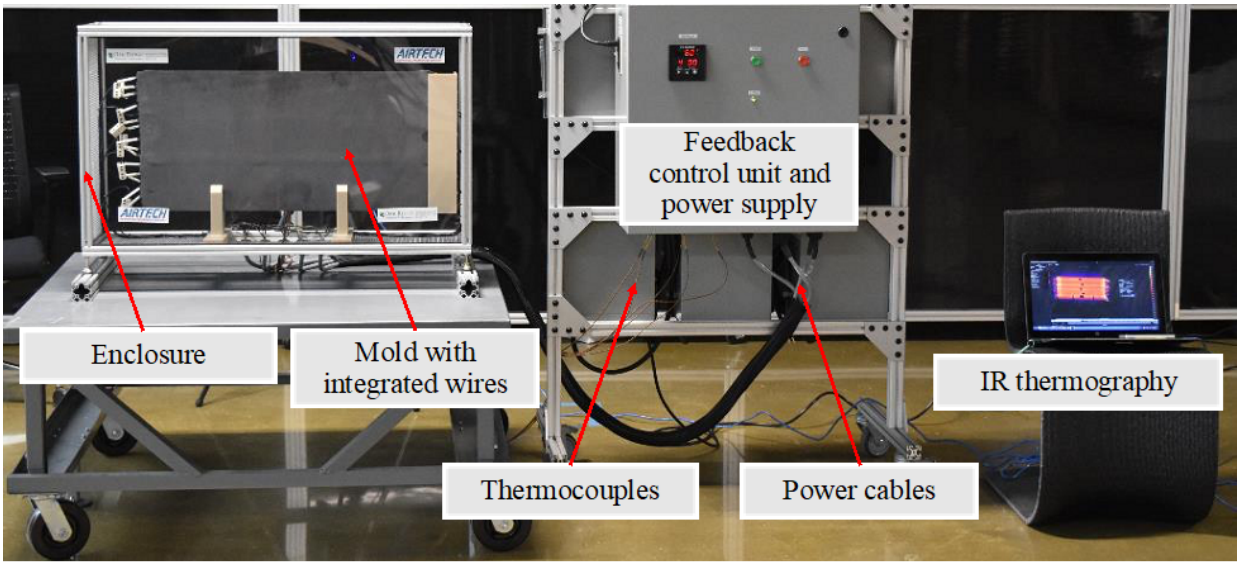

(a)

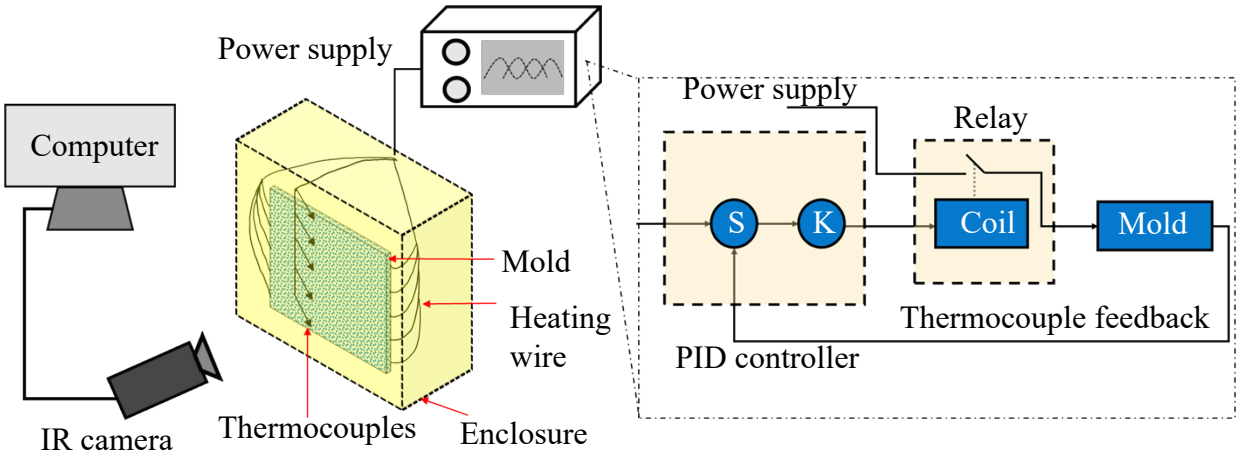

(b)

Figure 4. (a) Testing setup, power supply and control unit for testing the self-heated molds, and (b) schematic diagram of feedback control system of custom-made power supply for thermal testing of wire embedded mold. S and K represents the setpoint temperature for each zone and error, respectively.

3. Result

3.1 Tensile Testing

The tensile testing results of the neat and wire-embedded composite specimens are presented in Figure 5. In general, specimens showed a higher mechanical strength along the X-direction, compared to the Z-direction. In the case of the neat PC/CF composite specimen, excellent mechanical strength was found. When comparing to the 3D-printed polycarbonate plastic (64 MPa), the average ultimate tensile stress of the PC/CF composite along the X-direction, i.e. the direction of extrusion, was increased by 64% (105 MPa) [23]. When the nichrome wire was introduced within the PC/CF composite, the mechanical performance (UTS and modulus of elasticity) was slightly reduced in both the X and Z directions, compared to the neat specimen. The average UTS of the wire-embedded PC/CF was decreased by 17% along X-direction, compared to the neat PC/CF specimens as shown in Figure 5 (a). This was attributed to (i) increased inner-bead porosity within the deposited bead due to the wire co-extrusion and (ii) poor wetting/adhesion between wire and composite; thus, the load was partially transferred to the wires via the printed composite. These reasons are reported and explained with visual images in the optical imaging section. Two samples statistical t-test was performed as listed in Table 3 to compare the mean of PC/CF and PC/CG specimens. Null hypothesis (mean of sample 1, $\mu_1 =$ mean of sample2, μ_2) was rejected for the UTS of PC/CF in X direction as the P value is 0.00001 (less than 0.05).

Identical mechanical strength behavior was noticed in Z-direction, i.e., the average UTS value was reduced by 18% (from 13 MPa of Neat-Z to 11 MPa of Wire-Z). The null hypothesis was not rejected as the P value was 0.07636 and greater than 0.05. It was also observed that the average UTS value in the Z-direction (12 MPa) was significantly smaller than the X-direction (105 MPa). This behavior clearly demonstrated the inherent anisotropic mechanical properties of the AM fiber-reinforced part. In the case of large-scale extrusion AM, this anisotropic behavior can be ascribed to the fibers orientating along the direction of extrusion and to the impeded polymer chain diffusion between adjacent beads, also known as interlayer bonding [20], [24]–[26].

In the case of the wire-embedded PC/GF specimens, the average UTS value along X-direction was decreased by just 3%, compared to the neat specimen (from 72.77 MPa to 70.38 MPa), Figure 5 (b). In the Z-direction, the average UTS of both neat and wire-embedded PC/GF specimens was higher than that of the respective PC/CF specimens. The stiffness of chopped CF-based composites

is relatively high compared to that of GF-based composites, as has been previously reported for composites such as polypropylene [27] and polyamide-6 [28]. Similar stiffness behavior was noticed for both PC/CF and PC/GF specimens. The stiffer CF based specimens had less polymer diffusion at the bead interface due to the impeded polymer chain along extrusion direction compared to the PC/GF specimens. Analogous performance of the impeded chain mobility in CF and GF reinforced ABS composites were characterized via dynamic mechanical analysis and thermomechanical analysis [20].

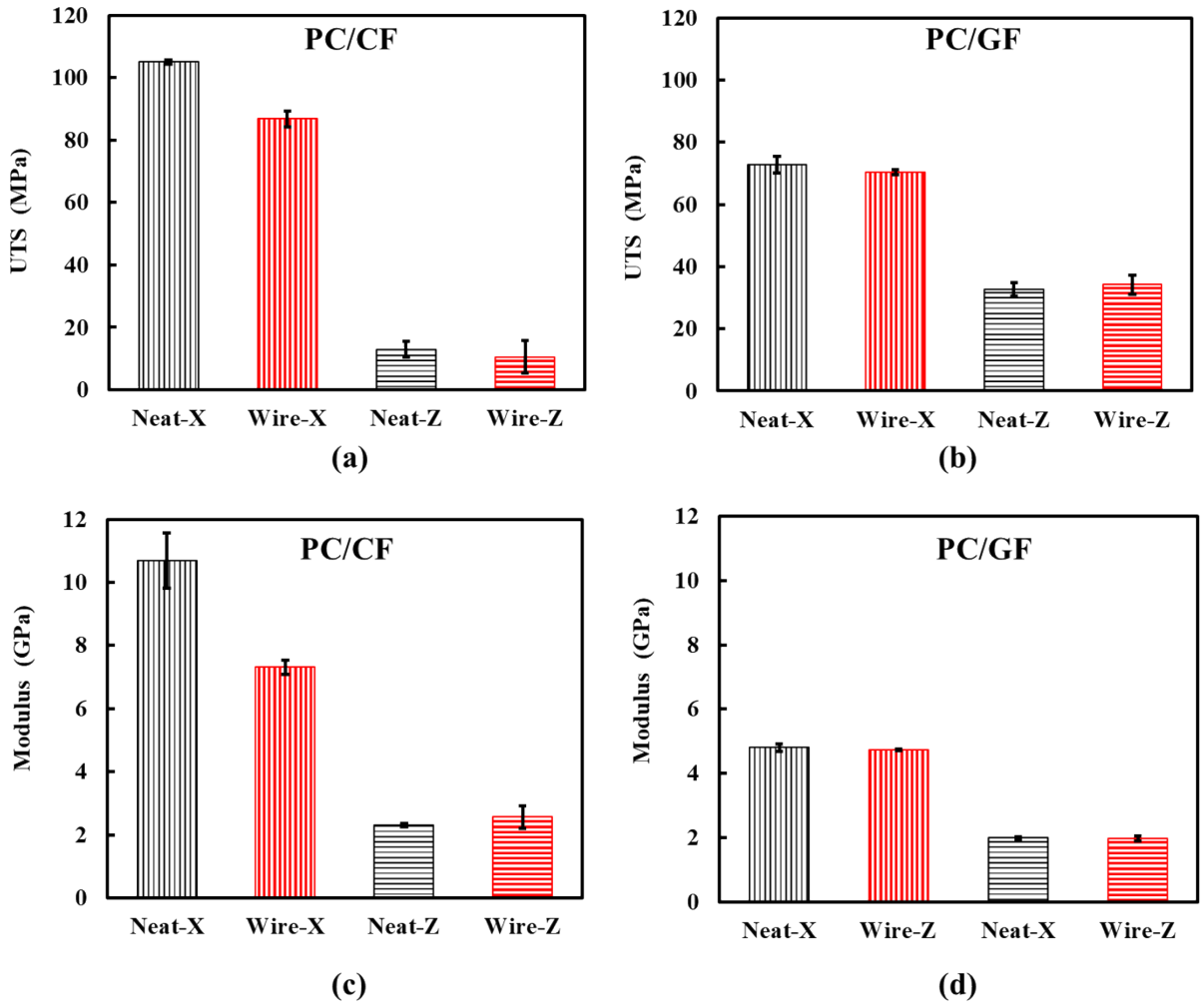

Figure 5. Tensile testing results of neat versus wire-embedded specimens for PC/CF and PC/GF composites; (a) Ultimate tensile stress (UTS) for PC/CF composite, (b) UTS for PC/GF composite, (c) Modulus of elasticity of PC/CF, and (d) Modulus of elasticity of PC/GF. Each bar

represents the average of at least five specimens and the error bars represent ± one standard deviation.

For tooling applications, stiffness, or the modulus of elasticity, is the most crucial mechanical property of the tooling material. In Figure 5 (c) and (d), an impact of the embedded wire within the composite specimen was noticed. In X-direction, the average modulus of elasticity of the PC/CF and PC/GF wire-embedded specimens was reduced by 31% and 2%, respectively, compared to the neat specimens. Like the trend observed in the UTS properties, the decrease in the modulus of elasticity for the PC/CF specimen in the X-direction was relatively high compared to the PC/GF specimen. By contrast, in the Z-direction, the average modulus of elasticity of the wire-embedded PC/CF and PC/GF specimens was increased by 10% and 1%, respectively, when compared to the neat specimens. According to the t-test analysis Table 3, there was no significant differences in the modulus of neat and wire embedded PC/GF specimens. Therefore, the mechanical properties of the PC/GF based composite samples were impacted relatively less than the PC/CF samples.

Table 3. Two sample t-test statistical analysis of tensile properties of PC/CF and PC/GF composites

PC/CF								
Tensile properties	Group 1			Group 2			t stat	P value
	Specimen	Mean	Std. Dev.	Specimen	Mean	Std. Dev.		
UTS (MPa)	Neat - X	105.10	0.66	Wire -X	86.84	2.65	17.97	0.00001
	Neat - Z	12.93	2.55	Wire -Z	10.54	5.28	1.43	0.07636
Modulus (GPa)	Neat - X	10.69	0.87	Wire -X	7.31	0.22	8.43	0.00001
	Neat - Z	2.31	0.06	Wire -Z	2.57	0.35	-1.15	0.12507
PC/GF								
UTS (MPa)	Neat - X	72.78	2.76	Wire -X	70.39	0.74	1.86	0.03106
	Neat - Z	32.75	2.15	Wire -Z	34.26	3.10	-0.89	0.18539
Modulus (GPa)	Neat - X	4.80	0.13	Wire -X	4.73	0.03	1.16	0.12312
	Neat - Z	1.99	0.04	Wire -Z	1.97	0.08	0.57	0.28274

3.2 Flexural Testing

Figure 6 (a) shows the average flexural stresses of the neat and wire-embedded PC/CF specimens. In X-direction, the average flexural stress of the wire-embedded PC/CF was reduced by 14% (159 MPa to 137 MPa) compared to the neat specimen. In the Z-direction, the average flexural stress of wire-embedded specimen (59 MPa) remained almost the same as a neat specimen (60 MPa). Two samples statistical t-test analysis with null hypothesis (mean of sample 1, $\mu_1 =$ mean of sample2, μ_2) results are listed in Table 4. The average value of the flexural stress was significantly different in X-direction thus the null hypothesis was rejected. However, higher P value in Z-direction ($0.30188 > 0.05$) implied that there was no significant difference between the mean of neat and wire embedded PC/CF specimens. Similar to the tensile strength of large-scale printed parts, anisotropy remained an inherent property of the flexural strength. For the PC/GF specimens, as shown in Figure 6 (b), the average flexural stress of the neat specimen in the X-direction was 118 MPa, while that of the wire-embedded specimen was reduced to 109 MPa, i.e., it was decreased by 8%. In the Z-direction, the average flexural stress of the neat specimen was 63 MPa and that of the wire-embedded specimen was 60 MPa i.e., it was decreased by less than 5%. Flexural stress of PC/GF specimens in both directions were significantly different as the P value was less than the 0.05.

The flexural modulus behavior was similar to the trends of the flexural stresses for both the PC/CF and PC/GF composites. However, the mean value of modulus in all samples were significantly different as the null hypothesis was rejected due to the lower P values as listed in Table 4. For the PC/CF specimens, the average modulus of the wire embedded-specimen in the X-direction (7 GPa) was 30% lower than that of the neat specimen (10 GPa), as shown in Figure 6 (c). In Z-direction, the average modulus of the wire-embedded specimens (2.35 GPa) was less than 5% lower than that of the neat specimen (2.47 GPa). In PC/GF composite as shown in Figure 6 (d), the average modulus of the wire embedded specimen was reduced by 13% in X-direction and 12% in Z-direction compared to the corresponding neat specimens. While comparing the modulus between CF and GF based composite, it was noticed the average modulus of both neat and wire embedded PC/CF specimen was almost doubled than the PC/GF specimen in X-direction. However, in Z-direction, an almost similar value of the modulus was noticed in all specimens because of the anisotropy in the printed part.

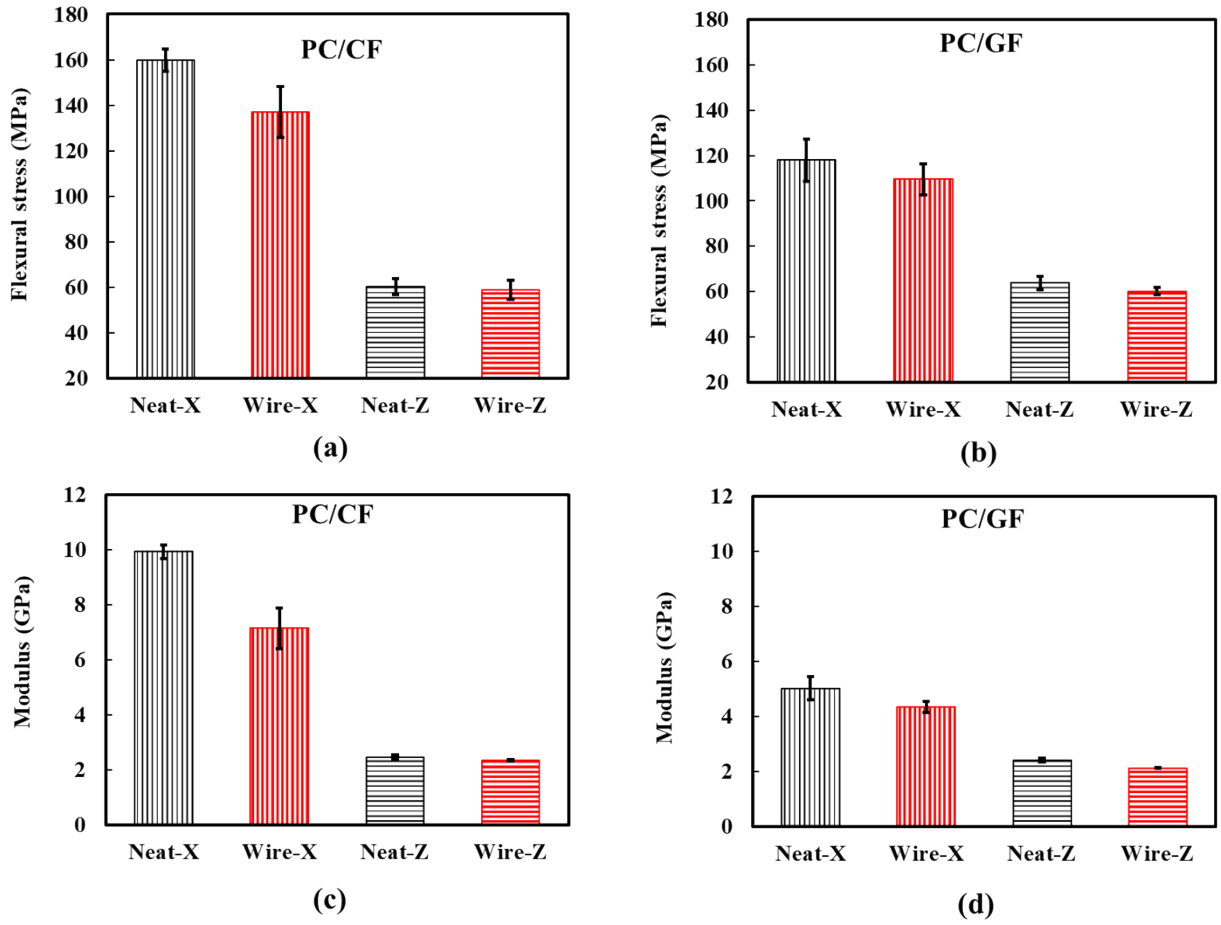

Figure 6. Flexural testing results of neat versus wire-embedded specimens; (a) Flexural stress of PC/CF composite, (b) Flexural stress for PC/GF composite, (c) Flexural modulus of PC/CF, and (d) Flexural modulus of PC/GF. Each bar represents the average of at least five specimens and the error bars represent ± one standard deviation.

Table 4. Two sample t-test *statistical analysis of flexural properties of PC/CF and PC/GF composites*

PC/CF								
Flexural properties	Group 1			Group 2			t stat	P value
	Specimen	Mean	Std. Dev.	Specimen	Mean	Std. Dev.		
Stress (MPa)	Neat - X	159.92	4.92	Wire -X	137.07	11.30	4.14	0.00001
	Neat - Z	60.29	3.50	Wire -Z	59.03	4.15	0.51	0.30188
Modulus (GPa)	Neat - X	9.93	0.24	Wire -X	7.15	0.74	7.95	0.00001
	Neat - Z	2.47	0.07	Wire -Z	2.35	0.03	3.92	0.00004
PC/GF								
Stress (MPa)	Neat - X	118.06	9.31	Wire -X	109.49	6.80	1.67	0.04746
	Neat - Z	63.79	3.00	Wire -Z	60.21	1.61	2.35	0.00938
Modulus (GPa)	Neat - X	5.02	0.42	Wire -X	4.35	0.21	3.21	0.00066
	Neat - Z	2.42	0.08	Wire -Z	2.12	0.01	8.47	0.00001

3.3 Microscopic Image Analysis

Inter-bead mesostructured porosity is an inherent characteristic property of extrusion-based additive manufacturing [29]. While a part 3D printed with neat material contains only the inter-bead porosity, fiber-reinforced composite materials have intra-bead porosity as well. Figure 7 (a) and (b) show representative optical images of sectioned wire-embedded PC/CF and PC/GF samples, respectively. Zoomed-in portions of those images are shown in Figure 7 (c) and (d) to better show the intra-bead voids found in wire-embedded PC/CF and PC/GF specimens, respectively. These voids were generated within the bead for the following reasons: (a) the screw-driven extruder did not have a venting system, so the air entrapped within the pellet feedstock formed voids within the extruded bead, (b)voids formed at the edge or around the chopped fiber reinforcements because the two phases (polymer and fiber) flow independently during melt extrusion printing [30], and (c) co-extrusion of the wires led to interfacial gaps between the wire and the surrounding composites. As expected, the voids impacted the mechanical performance of both composites by developing stress concentration points within the beads.

Another source of the reduced mechanical performance of both composites, particularly in the extrusion direction (X-axis), was the embedded nichrome wire. Note that the embedded nichrome wire was used in the co-extrusion printing without any surface treatment or modification. It was

expected that, together, the intra-bead voids and untreated nichrome wire would reduce the mechanical properties. Figure 8 (a) shows the gauge section of a fractured PC/CF tensile sample in the X-direction, after testing. It can be noticed that the sample was fractured across the composite while the wires were still intact (undamaged) and partial load transfer occurred between the composite and the wires. Figure 8 (b) and (c) show representative SEM images of the tensile specimen fractured surfaces of PC/CF and PC/GF specimens, respectively. An interfacial gap surrounding the wire was generated in both composite specimens. It is suspected that this interfacial gap was created due to the accumulation of intra-bead voids and poor wetting between the polymer matrix and wire surface. The impact of the interfacial gap on the tensile and flexural properties was clearly observed; therefore, surface modification of the embedded wire is necessary, to improve the wetting and interfacial adhesion between the co-extruded wire and the printed composite.

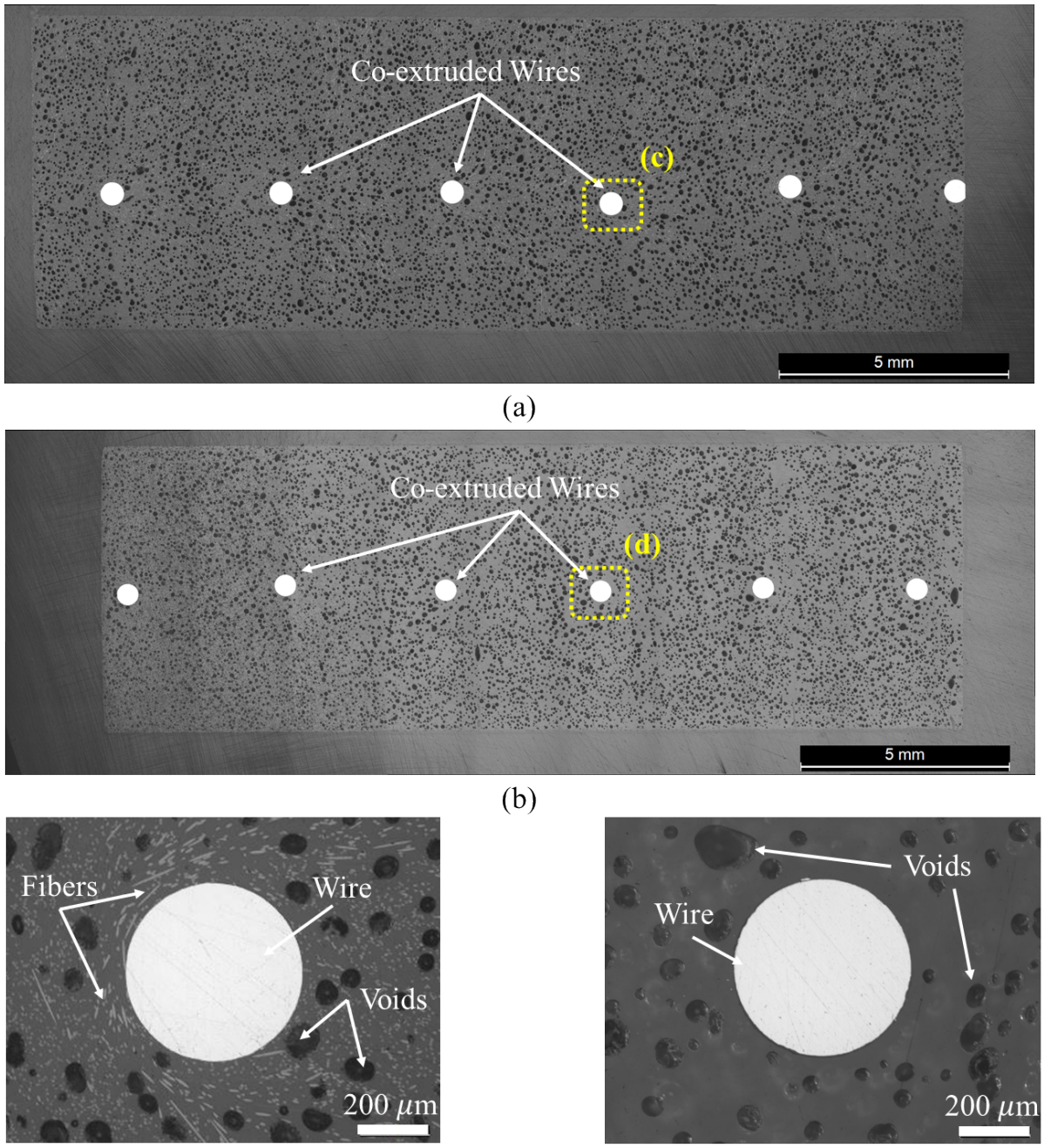

Figure 7: Optical microscopy images for a cross-section of the co-extruded wire specimens; (a) overall view for the PC/CF sample showing the integrated co-extruded wires, (b) Overall view for the PC/GF sample showing the integrated co-extruded wires, (c) Zoom in image for the PC/CF samples showing wire-composite interface, micro-voids and fibers, and (d) Zoom in image for the PC/GF samples showing wire-composite interface, micro-voids, and fibers.

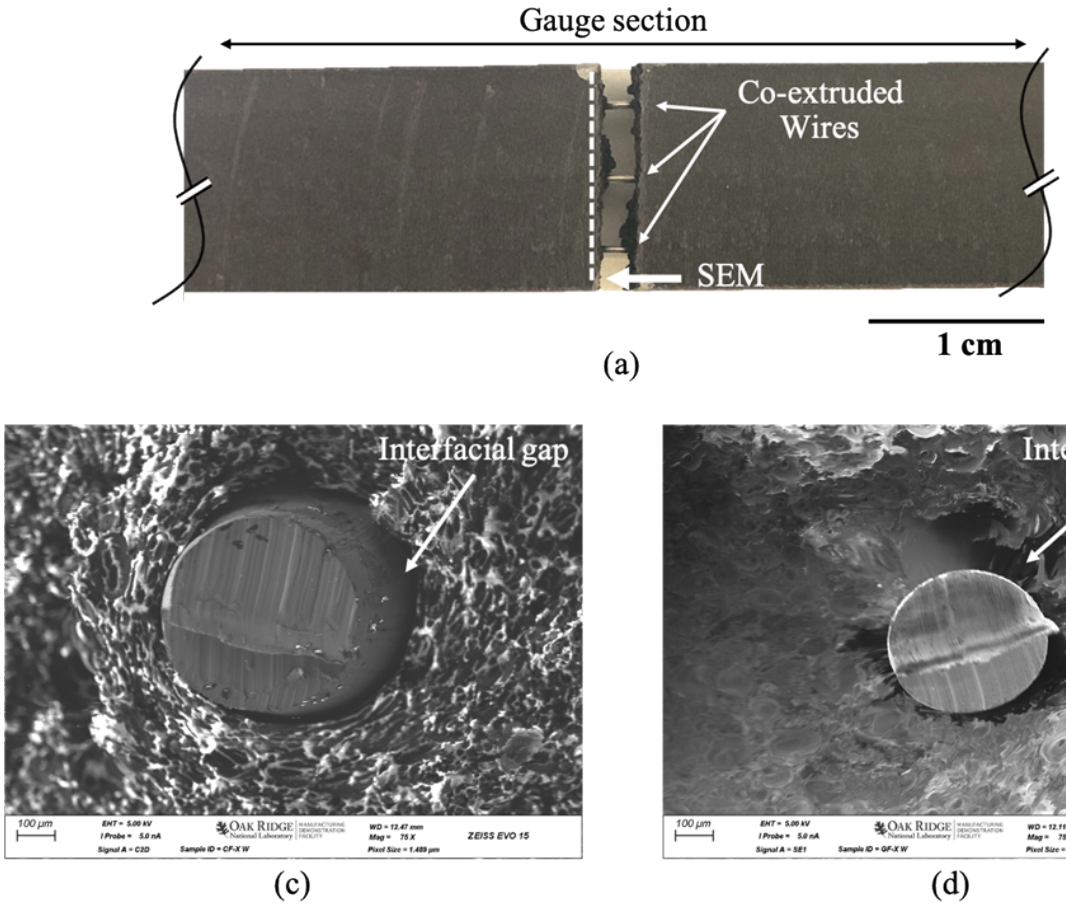

Figure 8 (a) Fractured PC/CF sample in the X-direction after tensile testing, (b) SEM image of fracture surface of a representative PC/CF tensile specimen, and (c) SEM image of fracture surface of a representative PC/GF tensile specimen. The micrographs demonstrate the interfacial gap between wires and the printed composite.

3.4 Thermal Testing of the Self-Heated Molds

Figure 9 (a) and (b) present the temperature distribution on the surfaces of the flat mold panels of the PC/CF and PC/GF composites, respectively. The goal of the thermal testing was to determine the temperature distribution and uniformity across the surface of the mold panel. In both cases, the temperature distribution was almost uniform at the steady-state condition. Note that Cursor 1 and 13 are outside of the effective heating zone. Therefore, Cursor 2 to Cursor 12 represent the actual temperature distribution over the mold surface. During the thermal testing of both molds, slight differences in temperature distribution within the effective area were noticed. Some hot spots and

cold spots were noticed in both panels throughout the thermal testing. In these locations, the embedded wires were skewed, i.e., during the manufacturing of the mold, the wires were not co-extruded exactly in the middle of the layer. Also, the distance between the surface and embedded wires was reduced after machining for surface finishing, which introduced the hot spots. In the case of the cold spots, it was noticed that embedded wires were missing in some layers due to breakage of the wire.

As mentioned in the experimental setup section, thermal testing was performed using a custom-made controller. The impact of the active feedback control system can be clearly seen in Figure 9 (c) and (d). Precise control of the temperature profile over the mold surface was possible due to the feedback-controlled power supply. To better understand the impact of the feedback control system in the mold panel heating, Figure 9 (e) and (f) plot the test data before and after the controller adjusted of the current flow in each heating zone.

In the case of the PC/CF mold, shown in Figure 9 (e), for the first hour of testing the temperature gradient on the mold surface was relatively high (from 92°C to 107°C) i.e., the difference across the mold surface was ±15°C. In the second hour, the current flow was adjusted manually in each zone using the controller by acquiring the temperature from IR thermography. The temperature gradient was then reduced to ±5°C (from 99°C to 104°C), with exception to Cursor 11, where the heating wire was missing.

For the PC/GF panel, shown in Figure 9 (f), steady state temperatures were obtained from Cursor 3 to Cursor 11 during the first hour of testing. Cursor 3 showed the maximum temperature of 100°C, while the Cursor 9 and Cursor 11 showed the minimum temperature of 90°C. Thus, the temperature difference between the hot and cold spots in the steady state condition was 10°C. During the second hour of testing, the current flow was adjusted using the controller and IR thermography. A steady state temperature profile of the mold was obtained, and the temperature difference was only 5°C between the hot and cold spot. Manual adjustment of the power supply during the second hour of testing led the temperature to increase at Cursor 9 and Cursor 11, from 90°C to 95°C, and minimized the temperature gradient within the mold surface.

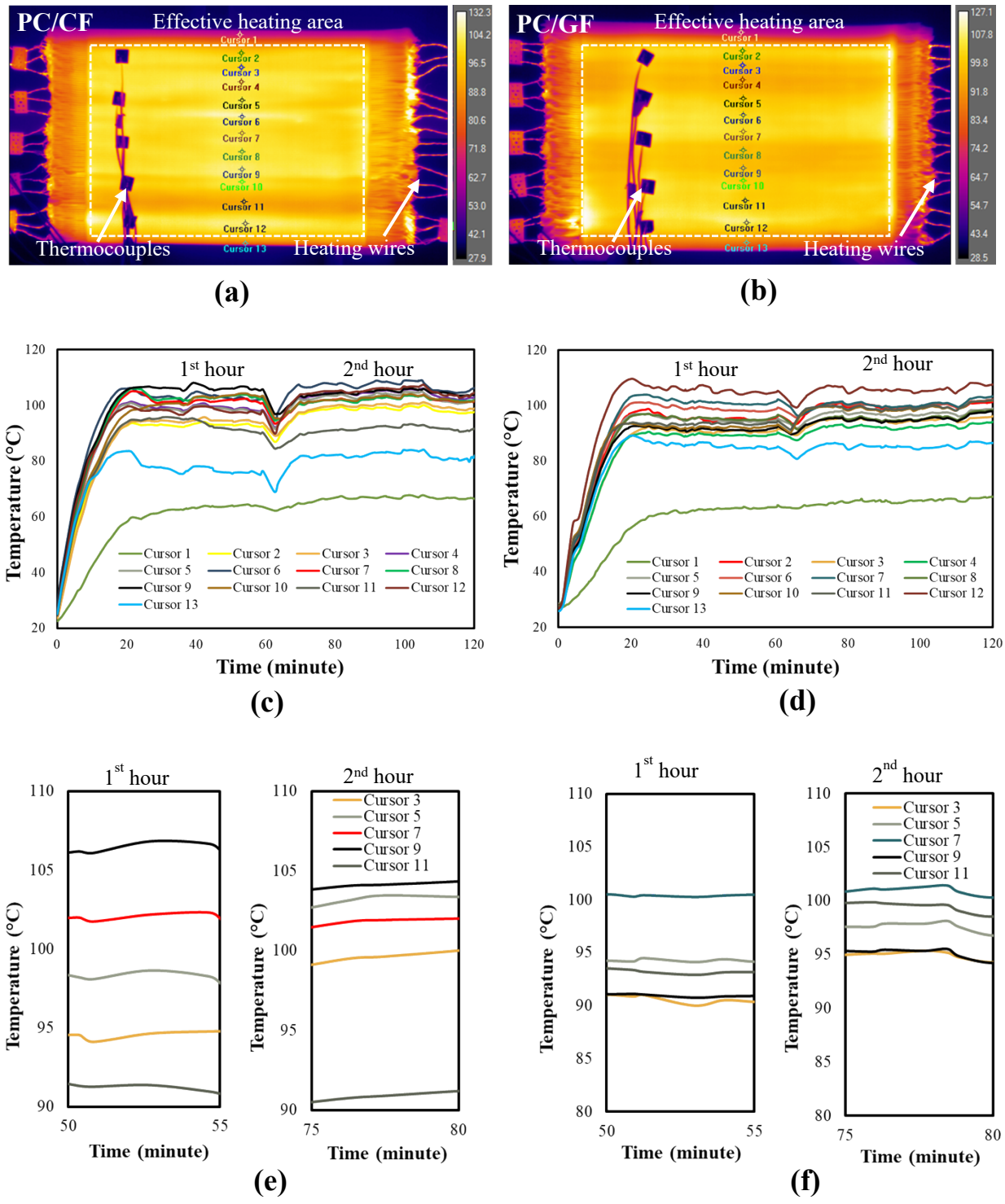

Figure 9. Representative temperature field (°C) of self-heated molds via IR thermography while active feedback control system was used; (a) PC/CF mold, and (b) PC/GF mold. Temperature distribution of the mold surface was analyzed as a function of time, (c) PC/CF mold and (d)

PC/GF mold. Temperature distribution in first and second hour of testing to determine the effectiveness of the control system in achieving uniform heating profile for, (e) PC/CF mold, and (f) PC/GF mold.

4. Discussion

Self-heated mold fabrication via a large-scale AM machine with an integrated wire coextrusion tool required a significant amount of post-processing work. Several wires were broken during the post-processing operations, which included material removal from each end of the embedded wire within the molds, machining, and specimen harvesting. Thus, thermal testing results showed cold spots within the mold parts. Currently a Generation-2 wire coextrusion system is under development, and initial lab trials showed that all the drawbacks of Generation-1 can be overcome with new design modifications. Wire placement within the bead has improved the accuracy and reliability of the coextrusion system up to 95%. In addition, the wire anchoring mechanism during the printing is modified thus reduces the use of sacrificial parts and materials. The details of the new design modifications are not within the scope of this work and authors envisioned to pursue a publication in future.

We also noticed that embedding heating wires within each of the beads was time-consuming and it could be optimized by skipping wires in some layers. A similar investigation was performed on small-scale coupons, in which the 3D-printed polycarbonate substrate was embedded with copper wire to demonstrate the resistance heating and thermal profile [31]. Three different embedding configurations showed that the wire could be skipped to obtain high temperature surfaces. However, the convection cooling in the air increases the power requirement. Thus, the authors envisioned fabricating a mold with fewer embedded wires (~50%), achieving a uniform temperature profile on one of the surfaces of mold while the other surfaces would be insulated to reduce the convection cooling as well as optimize the overall cost.

We fabricated two different composite molds using PC/CF and PC/GF pellet feedstock. Both composites showed improved mechanical properties compared to neat polycarbonate plastic counterparts, however, the PC/CF specimens showed relatively high anisotropy compared to the PC/GF specimens. It is suspected that the higher heat capacity and thermal conductivity of the PC/CF led to faster cooling of the 3D printed beads during the printing process compared to the PC/GF composite. Faster cooling impeded the interlayer bonding and wettability of PC/CF

composite, thus increasing the anisotropy in the mechanical properties. For thermal testing, both composite molds were heated up to 100°C and maintained uniform temperature profiles.

It is worth noting that a relatively low-cost mold can be fabricated using a GF-reinforced composite, as it provided sound mechanical properties and thermal testing results. To the economical aspect of the large-scale 3D printing, the cost associated with the PC/CF mold was relatively high compared to the PC/GF mold. Therefore, 3D printing large scale mold structures with GF-based composites is an area of interest. However, attention need to be considered for the reduced dimensional stability during the printing process associated with the relativity higher Coefficient of Thermal Expansion (CTE) of the GF.

5. Conclusion

A custom-made, integrated wire co-extrusion tool was made on the BAAM system at ORNL to manufacture composite molds using two different composites. Wire-embedded composite molds were tested to determine the temperature distribution over the mold panels. Thermal testing results indicated a promising application toward OOA tooling. The inherent anisotropy of the BAAM-printed parts was noticed, regardless of the material selection. In addition to the mesostructured inter-bead voids, intra-bead voids were formed, and together with the interfacial gap between wire and polymer composite, impacted the mechanical performance. When comparing between the PC/CF and PC/GF composites for OOA application, in terms of the operational temperature limit, the GF-based mold showed a promising result: it was possible to achieve identical uniform temperature distribution with a lower cost of materials compared to the CF-based composite, regardless of the mechanical anisotropy. In the future, further investigations will be focused on the use of a surface-modified heating wire to improve the adhesion between the polymer composite and the wire, which will ultimately improve the mechanical performance as well. In addition, the wire placement within the bead will be optimized; wire embedding will be done by skipping layers to reduce the number of wires within the printed part, while still achieving a similar temperature.

Acknowledgments

This research was supported by the DOE Office of Energy Efficiency and Renewable Energy (EERE), Advanced Manufacturing Office, and used resources at the Manufacturing Demonstration Facility, a DOE-EERE User Facility at Oak Ridge National Laboratory. This research was supported in part by an appointment to the Oak Ridge National Laboratory ASTRO Program, sponsored by the U.S. Department of Energy and administered by the Oak Ridge Institute for Science and Education.

For large scale additive manufacturing, the printing equipment was provided by Cincinnati Incorporated, a manufacturer of metal and additive manufacturing equipment, headquartered in Harrison, Ohio (www.e-ci.com).

The printing material was provided by Techmer PM, a material design and manufacture company headquartered in Clinton, TN.

References

[1] K. Friedrich and A. A. Almajid, “Manufacturing aspects of advanced polymer composites for automotive applications,” *Appl. Compos. Mater.*, vol. 20, no. 2, pp. 107–128, 2013, doi: 10.1007/s10443-012-9258-7.

[2] J. Holbery and D. Houston, “Natural-fiber-reinforced polymer composites in automotive applications,” *Jom*, vol. 58, no. 11, pp. 80–86, 2006, doi: 10.1007/s11837-006-0234-2.

[3] P. S. Veers *et al.*, “Trends in the design, manufacture and evaluation of wind turbine blades,” *Wind Energy*, vol. 6, no. 3, pp. 245–259, 2003, doi: 10.1002/we.90.

[4] “Manufacturing processes for composite materials and components for aerospace applications,” pp. 59–81, Jan. 2020, doi: 10.1016/b978-0-08-102679-3.00003-4.

[5] M. Torres, S. Piedra, S. Ledesma, C. A. Escalante-Velázquez, and G. Angelucci, “Manufacturing process of high performance-low cost composite structures for light sport aircrafts,” *Aerospace*, vol. 6, no. 2, 2019, doi: 10.3390/aerospace6020011.

[6] P. Hubert, G. Fernlund, and A. Poursartip, “Autoclave processing for composites,” in *Manufacturing Techniques for Polymer Matrix Composites (PMCs)*, Elsevier, 2012, pp. 414–434.

[7] A. R. Mallow and F. C. Campbell, “Autoclave Processing,” in *Processing of Composites*, München: Carl Hanser Verlag GmbH & Co. KG, 2000, pp. 293–316.

[8] “Boeing: ‘Grand-scale’ autoclave for Boeing’s biggest wings nears completion,” *Boeing*, 2015. https://www.boeing.com/company/about-bca/washington/grand-scale-autoclave-for-boeing-s-biggest-wings-nears-completion-06-16-2015.page (accessed Jan. 18, 2021).

[9] “Boeing: Second autoclave underway for Everett’s Composite Wing Center,” *Boeing*, 2018. https://www.boeing.com/company/about-bca/washington/cwc-777x-autoclave-05-10-18.page (accessed Jan. 18, 2021).

[10] A. A. Hassen, J. Lindahl, X. Chen, B. Post, L. Love, and V. Kunc, “Additive manufacturing of composite tooling using high temperature thermoplastic materials,” *Int. SAMPE Tech. Conf.*, vol. 2016-Janua, no. April 2018, 2016.

[11] A. W. Smith, K. Goyette, C. Kazanas, and P. Hubert, “Development of a heated tooling solution to improve process flexibility for out-of-autoclave prepregs,” *Int. SAMPE Tech. Conf.*, no. January 2013, 2013.

[12] D. Dixit, R. Pal, G. Kapoor, and M. Stabenau, “Lightweight composite materials processing,” in *Lightweight Ballistic Composites: Military and Law-Enforcement Applications: Second Edition*, Elsevier Inc., 2016, pp. 157–216.

[13] T. Centea, L. K. Grunenfelder, and S. R. Nutt, “A review of out-of-autoclave prepregs - Material properties, process phenomena, and manufacturing considerations,” *Composites Part A: Applied Science and Manufacturing*, vol. 70. Elsevier Ltd, pp. 132–154, Mar. 01, 2015, doi: 10.1016/j.compositesa.2014.09.029.

[14] A. A. Hassen *et al.*, “The durability of large-scale additive manufacturing composite molds,” in *CAMX Conference Proceedings. , September 26-29, 2016.*, 2016, no. April 2018, pp. 0–10.

[15] B. K. Post *et al.*, “Using Big Area Additive Manufacturing to directly manufacture a boat hull mould,” *Virtual Phys. Prototyp.*, vol. 14, no. 2, pp. 123–129, 2019, doi: 10.1080/17452759.2018.1532798.

[16] L. J. Love *et al.*, “The importance of carbon fiber to polymer additive manufacturing,” *J. Mater. Res.*, vol. 29, no. 17, pp. 1893–1898, 2014, doi: 10.1557/jmr.2014.212.

[17] A. A. H. Kazi Md Masum Billah, Jesse Heineman, Alex Roschli, Seokpum Kim, Gregory Haye, Vlastimil Kunc, “Integrated Wire Co-Extrusion Technology in Large Format Additive Manufacturing,” *Manuf. Lett.*, 2021.

[18] C. Atkins *et al.*, “Wire Co-Extrusion With Big Area Additive Manufacturing,” in *Solid Freeform Fabrication 2019: Proceedings of the 30th Annual International*, 2019, pp. 1549–1557.

[19] C. E. Duty *et al.*, “Structure and mechanical behavior of Big Area Additive Manufacturing (BAAM) materials,” *Rapid Prototyp. J.*, vol. 23, no. 1, pp. 181–189, 2017, doi: 10.1108/RPJ-12-2015-0183.

[20] K. Masum, F. A. R. Lorenzana, N. L. Martinez, R. B. Wicker, and D. Espalin,

"Thermomechanical characterization of short carbon fi ber and short glass fi ber-reinforced ABS used in large format additive manufacturing," *Addit. Manuf.*, vol. 35, no. April, p. 101299, 2020, doi: 10.1016/j.addma.2020.101299.

[21] A. Roschli *et al.*, "Designing for Big Area Additive Manufacturing," *Addit. Manuf.*, vol. 25, no. September 2018, pp. 275–285, 2019, doi: 10.1016/j.addma.2018.11.006.

[22] J. P. Joule, *The Scientific Papers of James Prescott Joule*, Volume 1. Cambridge Library Collection, 1984.

[23] M. Shojib Hossain, D. Espalin, J. Ramos, M. Perez, and R. Wicker, "Improved Mechanical Properties of Fused Deposition Modeling-Manufactured Parts Through Build Parameter Modifications," *J. Manuf. Sci. Eng.*, vol. 136, no. 6, p. 061002, 2014, doi: 10.1115/1.4028538.

[24] C. E. Duty *et al.*, "Structure and mechanical behavior of Big Area Additive Manufacturing (BAAM) materials," *Rapid Prototyp. J.*, vol. 23, no. 1, pp. 181–189, 2017, doi: 10.1108/RPJ-12-2015-0183.

[25] H. L. Tekinalp *et al.*, "Highly oriented carbon fiber-polymer composites via additive manufacturing," *Compos. Sci. Technol.*, vol. 105, pp. 144–150, 2014, doi: 10.1016/j.compscitech.2014.10.009.

[26] V. Kumar *et al.*, "High-performance molded composites using additively manufactured preforms with controlled fiber and pore morphology," *Addit. Manuf.*, vol. 37, p. 101733, Jan. 2021, doi: 10.1016/j.addma.2020.101733.

[27] S.-Y. Fu, B. Lauke, E. Mäder, C.-Y. Yue, and X. Hu, "Tensile properties of short-glass-fiber-and short-carbon-fiber-reinforced polypropylene composites." Accessed: Feb. 10, 2021. [Online]. Available: www.elsevier.com/locate/compositesa.

[28] S. H. Wu *et al.*, "Mechanical, thermal and morphological properties of glass fiber and carbon fiber reinforced polyamide-6 and polyamide-6/clay nanocomposites," *Mater. Lett.*, vol. 49, no. 6, pp. 327–333, 2001, doi: 10.1016/S0167-577X(00)00394-3.

[29] S. Wickramasinghe, T. Do, and P. Tran, "FDM-Based 3D printing of polymer and associated composite: A review on mechanical properties, defects and treatments,"

Polymers (Basel)., vol. 12, no. 7, pp. 1–42, 2020, doi: 10.3390/polym12071529.

[30] X. Jimenez Guzman, "Impact of Temperature and Screw Speed on Material Mesostructure and Tensile Strength in Large Area Pellet-fed Additive Manufacturing," University of Texas at El Paso, 2019.

[31] K. M. M. Billah, J. L. Corone, M. C. Halbig, R. B. Wicker, and D. Espalin, "Electrical and Thermal Characterization of 3D Printed Thermoplastic Parts with Embedded Wires for High Current-Carrying Applications," *IEEE Access*, vol. 7, pp. 1–1, 2019, doi: 10.1109/access.2019.2895620.